Journal of Geophysical Research: Space Physics

RESEARCH ARTICLE
10.1029/2017JA025161

Responses of Nitrogen Oxide to High-Speed Solar Wind Stream in the Polar Middle Atmosphere

Ji-Hee Lee[1], Geonhwa Jee[1,2], Young-Sil Kwak[3,4], Sang-bum Hong[1], Heejin Hwang[1], In-Sun Song[1], Young-Sook Lee[5], Esa Turunen[6], and Dae-Young Lee[7]

[1]Korea Polar Research Institute, Incheon, South Korea, [2]Department of Polar Science, Korea University of Science and Technology, Daejeon, South Korea, [3]Korea Astronomy and Space Science Institute, Daejeon, South Korea, [4]Department of Astronomy and Space Science, Korea University of Science and Technology, Daejeon, South Korea, [5]Department of Astronomy and Space Science, Chungnam National University, Daejeon, South Korea, [6]Sodankylä Geophysical Observatory, University of Oulu, Tähteläntie, Finland, [7]Department of Astronomy and Space Science, Chungbuk National University, Cheongju, South Korea

Abstract During high-speed solar wind stream (HSS) events, energetic electrons from the Earth's inner magnetosphere transfer solar wind energy to the high-latitude upper atmosphere, which may affect chemical compositions in the region. We conduct a study on the production of nitrogen oxides (NO_x) in the polar middle atmosphere by energetic electron precipitation (EEP) during HSS events in the period of international polar year 2007–2008 northern winter. During this period, the geomagnetic activity was generally quiet and there were no major solar events, which indicates that the EEPs were mostly associated with HSS events. The electron flux immediately increases with the onset of HSS events and remains elevated during the passage of the events. The estimation of the directly produced NO_x by EEPs was attempted by using the correlation between NO_x and dynamic tracers such as CO and CH_4. It was found that the direct effect of EEPs on NO_x reaches down to about 55-km altitude and the amount is estimated to be about 2 ppbv. This result indicates that the variations of polar stratospheric NO_x in winter are mostly associated with dynamical processes such as vertical transport and horizontal mixing. We also found that the middle atmospheric O_3 depletion during HSS events seems to be related to the EEP-induced NO_x at least in the uppermost stratosphere in the polar region.

Key Points:
- Direct effect of energetic electrons on NO_x during HSS events was evaluated
- EEP may directly affect NO_x down to about 55-km altitude in the polar winter hemisphere
- Ozone depletion at the altitude of 46–49 km may be associated with downward transported NO_x

Correspondence to:
G. Jee,
ghjee@kopri.re.kr

Citation:
Lee, J.-H., Jee, G., Kwak, Y.-S., Hong, S.-b., Hwang, H., Song, I.-S., et al. (2018). Responses of nitrogen oxide to high-speed solar wind stream in the polar middle atmosphere. *Journal of Geophysical Research: Space Physics*, *123*, 9788–9801. https://doi.org/10.1029/2017JA025161

Received 27 DEC 2017
Accepted 23 OCT 2018
Accepted article online 29 OCT 2018
Published online 22 NOV 2018

1. Introduction

Precipitating energetic electrons and protons (eV–MeV) from the Earth's magnetosphere are important sources of the production of nitrogen oxides, $NO_x = NO + NO_2$, in the polar middle and upper atmosphere. Precipitating energetic particles produce NO_x by colliding with the abundant molecular species (N_2 and O_2), which leads to excitation, dissociation, ionization, or dissociative ionization of these species and subsequent ion chemistry (Nieder et al., 2014; Porter et al., 1976; Rusch et al., 1981; Sinnhuber et al., 2012, 2013). The most of nitric oxide (NO) in the lower thermosphere, above 100 km, is directly produced by auroral electrons (1 eV to 10 keV) in the auroral oval (geomagnetic altitudes of 60–75°; Siskind et al., 1989; Solomon et al., 1999). In the mesosphere, NO_x can also be produced directly by energetic electrons. Medium-energy electrons (30–300 keV) deposit most of their energy in the upper mesosphere (75–100 km) to produce NO. Higher-energy electrons (0.1–1 MeV), associated with radiation belts, can penetrate down to 55–75 km (Lam et al., 2010; Meredith et al., 2011). In the lower thermosphere and upper mesosphere NO_x exists mainly in the form of NO, but below 70-km altitude it is converted to nitrogen dioxide (NO_2; Solomon et al., 1982). The stratospheric NO_x is attributed mainly to the oxidation of N_2O through the reaction with excited oxygen atoms ($O(^1D)$; McElroy & McConnell,1971). The N_2O is originating from the Earth's surface and photochemically destroyed in the upper stratosphere and is also a long-lived tracer in the stratosphere. The NO_x in the mesosphere and lower thermosphere can be transported down to the stratosphere by meridional circulation during polar winter when there is no photochemical destruction (Frederick & Orsini, 1982; Solomon et al., 1982). The descended NO_x can lead to changes in chemical composition throughout the stratosphere, which is the so-called *indirect effect* of energetic particles in the atmosphere.

Another important mechanism by particle precipitation is the formation of odd hydrogen, $HO_x = H + OH + HO_2$, from water vapor (H_2O) via positive ion chemistry involving water clusters

(Swider & Keneshea, 1973). This process is only effective below about 80-km altitude, where water vapor is enough (Andersson et al., 2012, 2014; Sinnhuber et al., 2012, 2013; Solomon et al., 1981). Below 80 km, however, HO_x is negligibly abundant because the chemical lifetime of HO_x is fairly short, 0.1–1 day at 75–80 km (Pickett et al., 2006).

It is well known that the existence of NO_x and HO_x in the middle atmosphere can significantly contribute to catalytic ozone destruction, which may have an appreciable effect on climate change (Rohen et al., 2005; Turunen et al., 2016; Verronen et al., 2005). For this reason, there are a number of previous studies on the chemical composition and temperature changes in the middle and upper atmosphere by solar proton event (SPE) and energetic electron precipitation (EEP) during geomagnetic storms. During the July 2000 SPE, NO_x was enhanced up to 50–100 ppbv at 65–70°N in the 55- to 70-km altitude region (Jackman et al., 2001). SPEs during the 2003 Halloween storm increased NO_x concentrations by 20–70 ppbv in the 40- to 60-km altitude region in the Arctic mean polar cap (>60°), which lasted for about 2 weeks (López-Puertas et al., 2005) and led to an ozone destruction of 20–60% over a period of several weeks (Seppälä et al., 2004). Verkhoglyadova et al. (2015) reported statistically significant increases of hydroxyl radicals (OH) density by SPEs at night. In the latitude region of 50–70°N, OH increased up to 5×10^6 cm^{-3} in the middle atmosphere, and corresponding nighttime ozone destructions of about 45% were observed.

The EEPs are mostly caused by energetic electrons originated from radiation belts during geomagnetic storms. Compared with SPEs, EEPs occur more frequently and persistently during high-speed (≥500 km/s) solar wind stream (HSS) events, and therefore, they can have more persistent impacts on the atmosphere (Andersson et al., 2014). The enhancements of NO by EEPs were observed at around 70- to 80-km altitude, and the mesospheric NO reached the level of 1.2 ppmv, or 2–3 orders of magnitude above the background level in Antarctica (Isono et al., 2014; Newnham et al., 2011). Funke et al. (2014) reported that oxidized nitrogen, NO_y (= $NO + NO_2 + HNO_3 + HNO_4 + ClONO_2 + 2(N_2O_5)$) concentration produced by EEPs was up to 1 ppmv in the winter solstice mesosphere, decreasing continuously with time and toward lower latitudes. They also found that NO_y induced by EEP contributes to catalytic ozone destruction in the middle and lower stratosphere, and the peak NO_y concentrations of a few ppbv are observed in spring even at as low as 22- to 25-km altitude, demonstrating a regular EEP impact on the entire stratosphere. On the other hand, EEP resulted in the enhancement of HO_x below about 80-km altitude (Sinnhuber et al., 2012; Solomon et al., 1981; Verronen & Lehmann, 2013), which was accompanied by ozone responses due to enhanced catalytic HO_x cycles at 60–80 km (Semeniuk et al., 2011). Verronen et al. (2005) also suggested that NO_x enhancement leads to HO_x repartitioning, which increases ozone loss by catalytic HO_x reactions, and EEP can have long-term, wintertime effects on mesospheric ozone.

The HSS events originating from solar coronal holes are maximized in the descending phases of the solar cycle, and they are associated with electron precipitation of broad energy range. However, it still remains uncertain whether the energetic electrons accompanied by HSSs make a significant contribution to the direct or indirect production of NO_x and HO_x budgets in the middle atmosphere when compared to their productions by SPEs or EEP events, with subsequent downward transport processes. Kirkwood et al. (2015) developed a model to simulate the effect of EEP during HSS events on the middle atmospheric NO, which has the potential to destroy stratospheric ozone. In this study, we investigate the atmospheric responses to HSSs in the Arctic winter using multiple satellite observations during the 2007–2008 period, which was the fourth international polar year (IPY 2007–2008). We utilized six HSS events from 6 November 2007 to 1 February 2008, which periodically occurred during three solar rotation periods but without any solar events such as coronal mass ejections or flares. In particular, we examine the altitude range of direct effects of EEP during HSS events on NO_x production in 2007–2008 polar winter. Also, analyzed are the Michelson Interferometer for Passive Atmospheric Sounding (MIPAS) measurements of stratospheric and mesospheric NO_x as well as the measurements of carbon monoxide (CO) and methane (CH_4) as a dynamic tracer in order to estimate the amount of directly produced NO_x ($NO + NO_2$). We also evaluate O_3 destruction by NO_x in the middle atmosphere during our study period. Finally, there was a sudden stratospheric warming (SSW) event at the end of the period, which provides us with the opportunity of investigating the effect of the EEP associated with HSS events during SSW event.

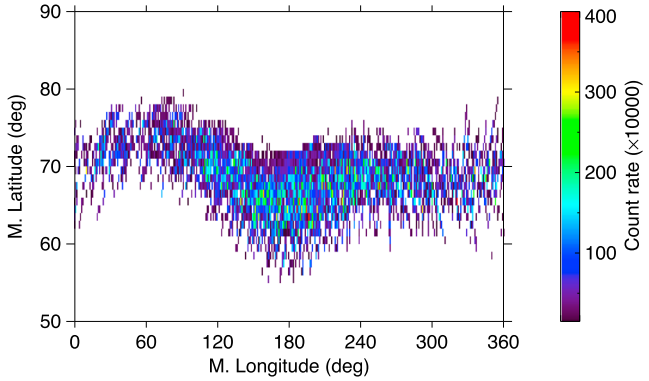

Figure 1. Distribution of energetic electrons (>30 keV) as a function of geomagnetic latitude and longitude in the Northern Hemisphere for the period of 6 November 2007 to 1 February 2008. The data are observed from the POES SEM/SEM-2 sensors in the 0° channel for the time period when recurrent high-speed solar wind streams occur. POES = Polar Orbiting Environmental Satellites; SEM = Space Environment Monitor.

2. Satellite Observations

2.1. Solar Wind Speed From Solar Wind Electron Proton Alpha Monitor/ACE

Advanced Composition Explorer (ACE) is a NASA Explorer mission to study the composition of matter including energetic particles from the solar wind, the other interplanetary medium, and other sources. The ACE spacecraft has been operated for about 20 years since it was launched on 25 August 1997 and stationed near the Earth-Sun First Lagrange Point (L1) on 12 December 1997. It carries nine instruments on board, six high-resolution sensors and three monitoring instruments to sample low-energy particles of solar origin and high-energy galactic particles. Solar Wind Electron Proton Alpha Monitor on board the satellite provides the information of low-speed streamer belt flows, high-speed solar wind, and other solar wind structures (McComas et al., 1998). For this study, we obtained the solar wind speed with 1 hr resolution from the Coordinated Data Analysis Web database (https://cdaweb.sci.gsfc.nasa.gov/index.html/).

2.2. Electron Flux From MEPED/POES

In this study, we use electron flux data from the Medium Energy Proton and Electron Detector (MEPED) on board the Polar Orbiting Environmental Satellites (POES) satellites. The POES satellite carries a suite of instruments that detect and monitor the influx of energetic ions and electrons into the atmosphere and the particle radiation environment at the satellite orbit altitude. POES is a low-altitude (800–850 km) orbiting satellite in the Sun-synchronous polar orbit with a period of ~100 min. Beginning with the NOAA-15 satellite, an upgraded version of the Space Environment Monitor (SEM-2) is being flown. For a detailed description of the SEM-2 instruments, see Evans and Greer (2004). SEM-2 includes MEPED and the Total Energy Detector. The MEPED has a set of solid-state energetic particle detectors that monitor the intensities of protons and electrons over the energy range extending from 30 keV to greater than 200 MeV. The solid-state detectors consist of 0° and 90° telescopes. The 0° telescope views outward along the Earth-center-to-satellite vector. Whenever the satellite is poleward of the geomagnetic latitude of about 33°, this detector monitors electrons in the bounce loss cone that will enter the Earth's atmosphere below the satellite (Rodger, Carson, et al., 2010). At lower latitudes, it measures geomagnetically trapped electrons. The observation of the 90° telescope is more complex; it tends to measure a combination of trapped and quasi-trapped electrons (i.e., electrons in the drift loss cone that are not lost to the atmosphere locally but are lost in regions where the magnetic field is weaker) at high latitudes, and it measures bounce loss cone electrons at low latitudes (Rodger, Clilverd, et al., 2010). We use data from the MEPED 0° electron telescope to monitor the electron precipitation in the high-latitude regions. First, SEM-2 data with 2-s time resolution were combined to produce daily mean electron counts at L shells of 4–20. These L values are equivalent to the geomagnetic latitudes of 60–77°. Here we focus primarily upon E1 (>30 keV electrons), E2 (>100 keV electrons), E3 (>300 keV electrons), and P6 (>6.9 MeV protons). The P6 channel detects >0.8-MeV electrons as well as >6.9-MeV protons with the same flux (Yahnin et al., 2016). Therefore, the P6 channel was used as 1-MeV electrons measurement. The geomagnetic latitudes of 60–77°N were selected from the latitudinal distribution of energetic electrons during HSS events in 2007–2008 winter periods as shown in Figure 1. This figure shows the distributions of electrons >30 keV in the Northern Hemisphere during the period of 6 November 2007 to 1 February 2008 in the geomagnetic latitude and longitude coordinate.

2.3. NO_x, CO, CH_4, and N_2O VMR From MIPAS/Environmental Satellite

The MIPAS is an Earth observation instrument on board the Environmental Satellite (Fischer et al., 2008). It was launched into a Sun-synchronous polar orbit at about 800-km altitude, with 14.4 orbits per day, on 1 March 2002. In April 2012, communication to the satellite was lost and no more MIPAS data are available since then. As an atmospheric sounder, MIPAS measures spectrally resolved limb radiance spectra in the midinfrared range from 4.1 to 14.7 μm (685–2,410 cm^{-1}) during day and night with global coverage from pole to pole, which can provide trace gas distributions also during the polar night. The extent of the

instantaneous field of view is 3 km in the vertical direction and 30 km in the horizontal direction. The instrument scanned the atmosphere most of the time in its nominal observation (NOM) mode, covering tangent altitudes from about 6 to 72 km.

In this study, we exploit nitrogen species of NO and NO_2, along with the transport tracers such as CO, CH_4, and N_2O. The data were from the observations taken in the NOM mode. The NO, NO_2, CO, CH_4, and N_2O data have been built from the following versions: V5R_NO_220, V5R_NO2_220, V4O_CO_200, V5R_CH4_224, V4O_N2O_201, and V5R_N2O_222. In the middle to high-latitude winters, typical vertical resolutions of NO_x are 4–6 km below 50 km and 6–9 km above the altitude, while the single-measurement precision is on the order of 5–15% (Funke et al., 2017). The vertical resolution of CO data is 6–12 km in the altitude range of 20–70 km. The single-measurement precision of CO is on the order of 20–30% above altitudes of 1 hPa to 70–80% in the lower stratosphere. The single-measurement precision of CH_4, having vertical resolution of 3–6 km, ranges from 10–20 ppbv in the upper stratosphere to 50–70 ppbv in the other altitude region. For this work, NO_x, CO, and CH_4 data have been filtered out using the visibility flag and diagonal values of the Averaging Kernel Matrix. In case of CH_4, we used only data within 2 sigma to exclude errors that were not removed. The N_2O data of vertical resolution are 3–6 km and have 10% level of precision. We use daily profiles of NO_x (NO + NO_2), CO, CH_4, and N_2O zonal mean values in the geomagnetic latitudes of 60–77°N. An interpolation was applied to the daily zonal mean of NO_x, CO, CH_4, and N_2O volume mixing ratio (VMR) when there is no observation for NOM mode.

2.4. O_3 VMR and Temperature From MLS/Aura

The Earth Observing System Microwave Limb Sounder (MLS) is one of four instruments on the NASA's Earth Observing System Aura satellite, launched on 15 July 2004. MLS instrument was placed into a Sun-synchronous orbit at about 705 km, to observe the atmosphere up to the latitude of 82°N/S (Waters et al., 2006). MLS measures thermal microwave emission, scanning from the ground to 90-km altitude with every 25 s for about 14.6 orbits per day to produce the global measurements of atmospheric composition, temperature, humidity and cloud ice.

The O_3 and temperature were obtained from Version 3.3 Level 2 data. The recommended useful vertical range of O_3 is from 261 to 0.0215 hPa with the vertical resolution of 2.5 to 6 km. The systematic error is typically less than 10%. The MLS temperature has vertical range of 261 to 0.001 hPa with vertical resolution of 3.6 to 6 km. For this work, O_3 and temperature data have been filtered out using the precision, status, quality, and convergence values (Livesey et al., 2011). The zonal mean values of daily O_3 VMR and temperature are utilized within the geomagnetic latitudes of 60–77°N as will be shown in the following section.

3. Results

3.1. Responses of NO to EEP During HSS Events in the Middle Atmosphere

During the period from 6 November 2007 to 1 February 2008 there were periodic stable HSS events due to three solar rotation cycles, while no solar eruptions like coronal mass ejections or flares were observed. These events also occurred around the declining phase of the solar cycle, in which HSSs occur more frequently and are being stronger. Figure 2a shows the hourly solar wind speed for this period. Strong HSSs occurred twice per each 27-day solar rotation with the maximum solar wind speed of 685 km/s. Figure 2b shows the daily electron flux with the energy of $>$30 (black line), $>$100 (green line), and $>$300 keV (magenta line) at the geomagnetic latitude of 60–77°N. The precipitating electron fluxes from medium to high energy observed by the POES satellite are almost simultaneously increased in association with the HSSs onset, and they remain elevated during the passage of HSSs. Figure 2c shows precipitating electron flux with the relativistic energy of $>$1 MeV, which is associated with the outer radiation belt. An important aspect of the relativistic electrons is that their flux levels appear to be governed by solar wind speed, and the flux levels are greatly enhanced during the HSS events (Blake et al., 1997; O'Brien et al., 2004). As can be seen in Figures 2b and 2c, the HSSs accompany the electrons in the Earth's magnetosphere and upper atmosphere with a broad range of energy. The HSSs are also associated with high-intensity long-duration continuous *AE* activity events (Tsurutani et al., 2004) and geomagnetic storms of the low to moderate levels as indicated by *Dst* index shown in Figure 2d.

For these HSS events, we investigate the responses of NO_x to EEP in the mesosphere and stratosphere. Figure 2e shows the temporal evolution of daily zonal mean NO VMR at the geomagnetic latitudes of 60–

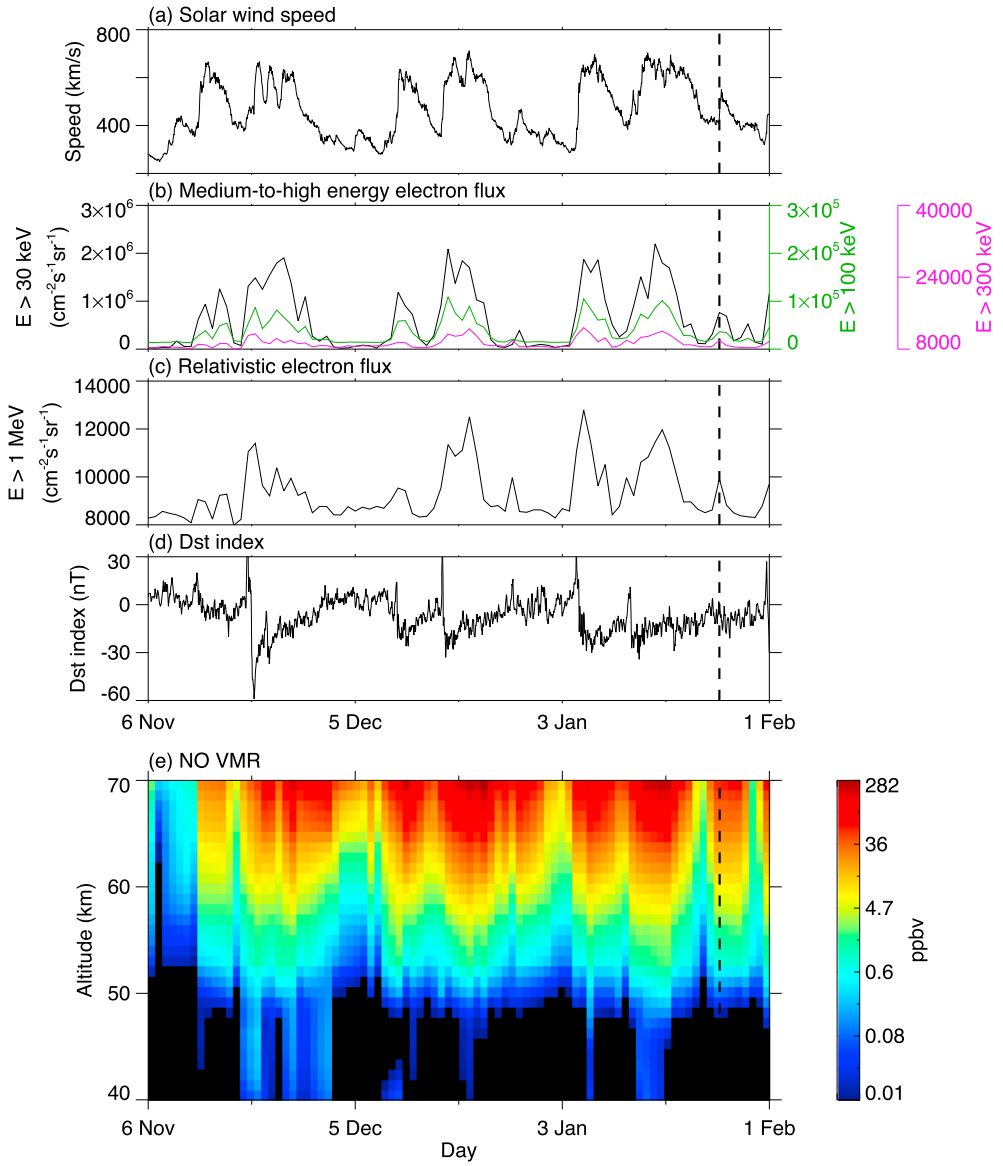

Figure 2. (a) High-speed solar wind stream events from 6 November 2007 to 1 February 2008; (b) daily mean of electron flux with the medium to high energy of >30 (black), >100 (green), and >300 keV (magenta) at the geomagnetic latitude of 60–77°N; (c) daily mean of relativistic electron flux with the energy >1 MeV at the geomagnetic latitude of 60–77°N; (d) the *Dst* index as a proxy for geomagnetic activity; and (e) the altitude profile of daily zonal mean NO VMR at the geomagnetic latitude of 60–77°N in the altitude range of 40–70 km. The black vertical dashed lines indicate the stratospheric sudden warming onset. VMR = volume mixing ratio.

77°N in the 40- to 70-km altitude range. It seems evident that NO directly responds to EEP during HSSs. The NO VMR enhances up to 282 ppbv at 70-km altitude on 23 December 2007, and it decreases with altitude and eventually disappears below about 50-km altitude. It should be noted that the daily variations of NO VMR are closely following the daily variations of solar wind speed or electron flux as shown in Figures 2a–2c.

3.2. Periodogram Analysis of NO Changes With Height During HSS Events

There have been a number of studies on the origin of mesospheric and stratospheric NO_x whether they show results from direct production of NO_x or downward transport of NO_x produced at higher altitudes during EEP or SPE events (Funke et al., 2007; Renard et al., 2006; Sinnhuber et al., 2014). Figure 2 indicates that the mesospheric NO seems to be closely related to precipitating electron flux during HSS events. In order to estimate

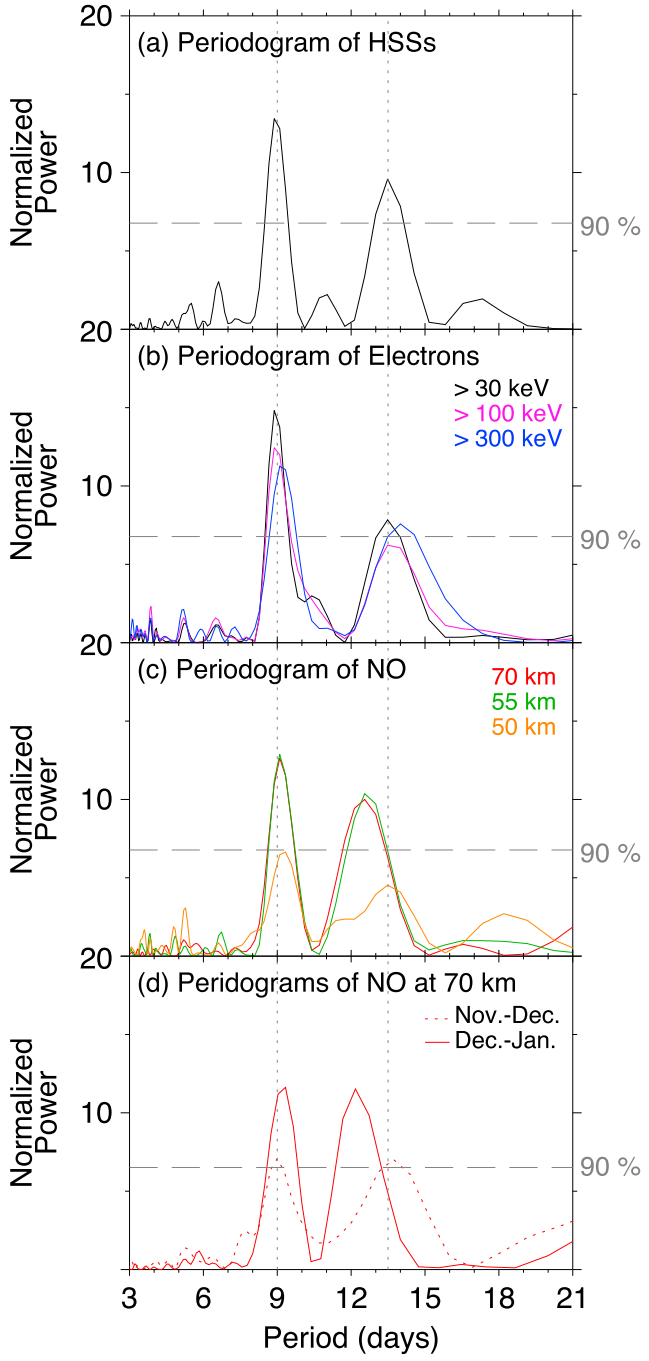

Figure 3. The power spectral densities from Lomb-Scargle periodogram analysis for (a) daily mean of solar wind speed; (b) daily mean of electron flux with the energy of >30 (black), >100 (magenta), and >300 keV (blue); (c) daily zonal mean of NO VMR at the altitudes of 50 (orange), 55 (green), and 70 km (red); and (d) daily zonal mean of NO VMR at 70 km for November–December (dashed line) and December–January (solid line) periods. The horizontal dashed lines indicate 90% significance level. HSS = high-speed solar wind stream; VMR = volume mixing ratio.

the vertical range of direct production of NO, we performed the Lomb-Scargle periodogram analysis for NO VMR, solar wind speed, and precipitating electron flux from 6 November 2007 to 1 February 2008 and presented the results of the analysis in Figure 3. The power spectral densities from Lomb-Scargle periodogram analysis are presented for daily mean values of (a) solar wind speed; (b) precipitating electron flux with the energy of >30 (black), >100 (magenta), and >300 keV (blue); and (c) NO VMR at the altitudes of 50 (orange), 55 (green), and 70 km (red). The horizontal dashed lines indicate 90% significance level. The power spectral density of solar wind speed in Figure 3a shows peaks at 9-day and 13.5-day periodicities above 90% significance level indicated by the horizontal dashed line. Previous studies reported that the solar wind speed has not only a periodicity of one 27-day solar rotation but also short-term periodicities of second (13.5-day), third (9-day), fourth (6.75-day), and fifth (5.4-day) harmonics (Gonzalez et al., 1993; Gonzalez & Gonzalez, 1987; Mursula & Zieger, 1996; Nayar et al., 2002). These short-term harmonics can be associated with the existence of solar coronal holes in relation to the solar rotation (Lei et al., 2008). The power spectral densities of precipitating electron flux show strong 9- and 13.5-day periodicities as in the solar wind speed. There are slight differences in the peaks of power spectral density among the energy levels of the electrons: both periodicities slightly deviate from the periods of HSS with increasing electron energy.

The spectral power densities of daily zonal mean NO VMR in Figure 3c have 9- and 12.5-day periodicities at the altitudes of 70 and 55 km. The 13.5-day periodicity of HSS and precipitating electron flux is shifted to a shorter period of 12.5 days for NO. At 50-km altitude, on the other hand, the power density of 9-day periodicity is on 90% significance level, which indicates that the direct response of NO by EEP during HSS events is effective down to 50-km altitude. Figure 3d shows the periodogram of daily zonal mean NO VMR for November to December (dotted line) and for December to January (solid line) at the altitude of 70 km. Note that NO VMR for December–January shows much shorter 12-day period while it shows 13.5-day period for November–December. The 12.5-day period in Figure 3c is the result of the combined effect of these two cases. The short 12-day period in December–January seems to be caused by severe depletion of NO_x due to the SSW event that occurred in January 2008, which will be discussed in the next section.

4. Discussions

4.1. Correlation Between Middle Atmospheric NO_x and Dynamical Tracers CO and CH_4

In winter when the NO_x chemical lifetime is in the range of few months, large amounts of lower thermospheric NO_x can gradually descend into the mesosphere and stratosphere within the polar vortex by the meridional circulation from summer to winter hemisphere (e.g., Funke et al., 2014; Randall et al., 2009). In order to estimate how much the direct production of NO_x by EEP during HSS events contribute to the middle atmospheric NO_x compared with the downward transport from the thermosphere, we investigate these processes by using dynamic tracers such as CO and CH_4. The principal source of CO in the middle atmosphere is the photolysis of carbon dioxide (CO_2) in the thermosphere in the summer hemisphere, and its subsequent meridional and vertical downward transports into the winter hemisphere. In the high-latitude winter hemisphere, the lifetime of CO is generally longer than a

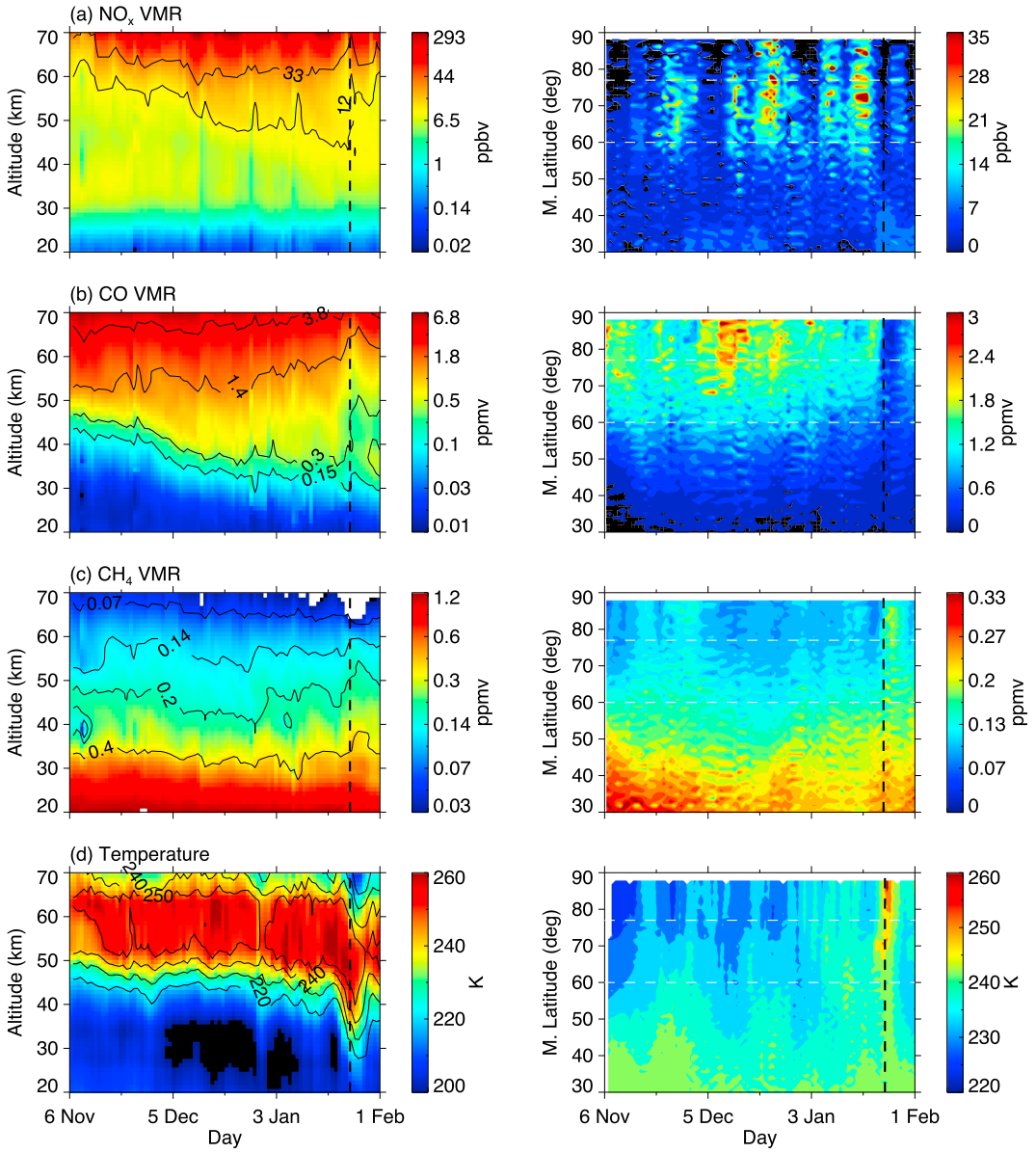

Figure 4. Vertical profiles of daily zonal mean VMRs and temperature in the geomagnetic latitude of 60–77°N (left panels) and the latitudinal variations of daily mean values in the altitude range of 40–70 km (right panels) for (a) NO_x, (b) CO, and (c) CH_4, and (d) temperature from 6 November 2007 to 1 February 2008. The black vertical dashed lines and white horizontal dashed lines indicate the stratospheric sudden warming onset and the geomagnetic latitude of 60° and 77°N, respectively. VMR = volume mixing ratio.

month (Minschwaner et al., 2010), which allows it to descend with air into the middle atmosphere within the polar vortex. In the middle atmosphere, therefore, NO_x and CO may show similar variations under the winter hemispheric meridional circulation, assuming only transport processes to determine NO_x VMR. On the other hand, the CH_4 shows quite a different altitude distribution from NO_x and CO; CH_4 is emitted at the Earth's surface and is transported upward into the higher altitudes. In the mesosphere, CH_4 also undergoes the destructive photolysis mainly by *Lyman-α* radiation in the summer hemisphere (Randall et al., 2007; Siskind & Russell, 1996). This CH_4-poor air is transported to the winter hemisphere by meridional circulation.

The left panels in Figure 4 show the height profiles of daily zonal mean VMRs of NO_x, CO, and CH_4 and daily zonal mean temperature in the geomagnetic latitude of 60–77°N from 6 November 2007 to 1 February 2008. The black vertical dashed line indicates the SSW onset time. We found in Figure 4a that NO_x during

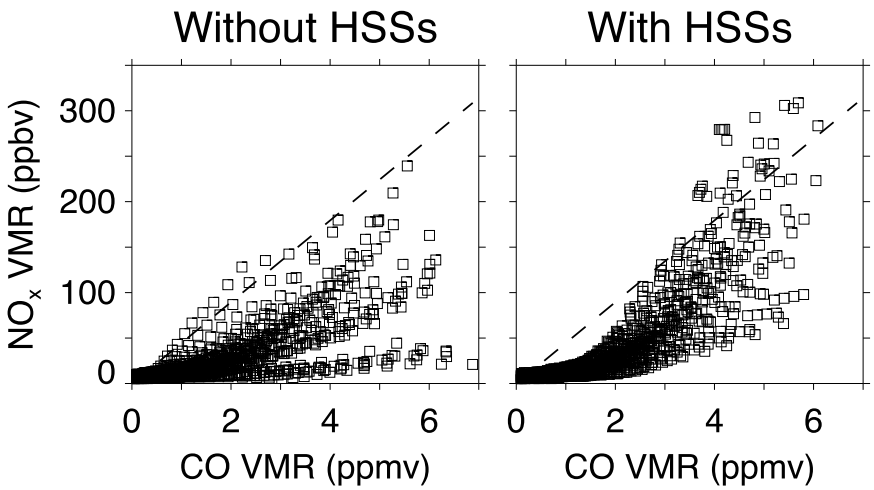

Figure 5. Scatterplots of NO_x and CO VMRs during the periods with and without HSSs in the altitude range of 20–70 km and the geomagnetic latitude of 60–77°N from 6 November 2007 to 1 February 2008. The black dashed lines indicate the secants of this distribution. VMR = volume mixing ratio; HSS = high-speed solar wind stream.

HSS events was clearly enhanced in the 60- to 70-km altitude. The enhanced NO_x then seems to be gradually transported downward throughout the period until the SSW occurred on 25 January 2008 (Wang & Alexander, 2009). The downwelling of NO_x seems to slow down at around the altitude of 45 km from the mid-December 2007 as the SSW onset approaches, although the mesospheric NO_x continues to be produced during HSS events. The CO VMR in the left panel of Figure 4b also shows similar temporal evolutions, but the overall downwelling tends to occur in the lower altitude region (i.e., in the stratosphere) than NO_x, and there seems to be no downwelling in the mesosphere since mid-December as the SSW onset approaches. Note that both NO_x and CO VMRs during SSW are different from before SSW: They are reduced with the onset of SSW in the altitude region above about 50 km for NO_x and above about 30 km for CO. The CH_4 VMR in the left panel of Figure 4c shows nearly opposite height profiles to NO_x and CO VMRs: the maximum values at the bottom almost linearly decrease with height. During SSW, the overall magnitude in the upper stratosphere is higher than before SSW, which is also opposite to NO_x and CO. The behaviors of these species may indicate that there are disturbances in the stratosphere and mesosphere during SSW, which must be related to the thermal and dynamical changes of the polar vortex in relation to SSW. The left panel of Figure 4d shows the temporal evolution of temperature. As SSW approaches, the warm layer in the lower mesosphere moves downward in January 2008 until the onset of SSW when the abrupt temperature change occurs.

In addition to the vertical downward transports, the horizontal mixing with the air from the lower latitudes can also be important to determine the abundances of the polar atmospheric species. To identify the horizontal mixing effect during HSSs, we present the mean VMRs for NO_x, CO, and CH_4, and temperature in the altitude range of 40–70 km from 6 November 2007 to 1 February 2008 at the right panels in Figure 4. The white dashed lines indicate the geomagnetic latitude of 60° and 77°N for the height profiles of the corresponding left panels. The NO_x VMR was clearly enhanced in the polar region above the geomagnetic latitude of about 60°N during HSS events. The right panels in Figures 4b–4d show the latitudinal distributions of CO and CH_4 and temperature. The mixing effects seem to be especially strong in the middle of November and at around the onset of SSW. Moreover, it seems that the strong horizontal mixing effects can also be found in the height distribution of the VMRs of CO and CH_4 in the same periods. These vertical and horizontal variations of NO_x, CO, and CH_4 have a good agreement. In the next section, we will attempt to estimate the directly produced NO_x by removing the contributions of the vertical and horizontal transports using the changes of the dynamic tracers.

4.2. Estimation of the Amount of Direct Production of NO_x

The height distributions of NO_x and CO are in a nonlinear relationship in the polar middle atmosphere because of their different vertical gradients. However, this relationship can be significantly disturbed if

there exist additional processes such as a direct local production of NO_x, photochemical loss of CO, or horizontal mixing effects by disturbed polar vortex. Figure 5 shows the scatterplots of NO_x versus CO VMRs in the altitude range of 20–70 km and in the geomagnetic latitude of 60–77°N with and without HSS for the period from 6 November 2007 to 1 February 2008. The dashed line depicts the secant of distribution of NO_x and CO VMRs. There are excess VMRs of NO_x across the secant for both with-HSS and without-HSS periods, but they are different. The excess NO_x with HSS is more significant and exists at higher altitudes than the excess NO_x without HSS. The latter may be generated from the horizontal mixing in relation to SSW in the absence of HSS. During HSS events, however, it may be caused by energetic electron-induced direct production. In this section, we investigated how much the direct production contributes to the NO_x VMR in the middle atmosphere during HSS events.

We attempt to estimate the transport and mixing effects on NO_x VMR by using the CO and CH_4 during the HSS events. Since the variations of CO and CH_4 in the middle atmosphere are assumed to be mainly caused by vertical transports and horizontal mixing without any direct production, they can represent the changes of mesospheric and stratospheric NO_x induced by transports and mixing. For direct comparison with NO_x and tracers, the CO and CH_4 VMRs must be converted to the vertical gradient of NO_x VMR. We first calculated the average height profiles of NO_x, CO, and CH_4 in the altitude range of 20–70 km from 6 November 2007 to 1 February 2008. Each height profile is the zonal mean in the geomagnetic latitude of 60–77°N. Then the ratio of daily height profiles of the tracer to the average profiles was multiplied by the average height profile of NO_x.

$$\text{Tracer}^{\text{cvt}} = \frac{\text{daily height profile of tracer}}{\text{average height profile of tracer}} \times \text{ average height profile of } NO_x. \quad (1)$$

The converted CO (CO^{cvt}) and CH_4 ($CH_4{}^{cvt}$) VMRs have similar height profiles to NO_x VMR. We calculate the changes (ΔX_i) of NO_x, CO^{cvt}, and $CH_4{}^{cvt}$ VMRs on a day (i) from the mean profiles ($\overline{X}_{0,i-1}$) during the period from 6 November to the day ($i-1$) as follows:

$$\Delta X_i = X_i - \overline{X}_{0,i-1} \quad (2)$$

Figure 6 shows the results of their mean profiles and the changes of NO_x, CO^{cvt}, and $CH_4{}^{cvt}$ VMRs. The estimated changes represent the variations of each species. The change of CO^{cvt} shows that there is a strong downward transport in the mesosphere in early November and early December and a modest downward transport in the stratosphere in December and January. While the variations of CO^{cvt} represent downward transports of the air, the variations of $CH_4{}^{cvt}$ represent the horizontal mixing effects on the polar middle atmosphere with the midlatitude region. We found that the horizontal mixing becomes remarkable in November and near SSW. The changes of CO^{cvt} and $CH_4{}^{cvt}$ in Figure 6 do not contain the transport effects of the directly produced NO_x in the middle atmosphere, which may be implied by different height distributions of NO_x and tracers, particularly CO^{cvt}, in the mean profiles. In order to take it into account in our estimation procedure, we also need to consider the changes of mean profiles of each species from the initial period before HSSs (not shown here). With all these information, we can estimate the amount of direct production of NO_x ($NO_x{}^{P}$) by subtracting these changes from ΔNO_x as follows:

$$NO_x{}^{P} \approx \Delta NO_x - \Delta CO^{cvt} - \Delta CH_4{}^{cvt} - \overline{\Delta NO_x} - \overline{\Delta CO^{cvt}} - \overline{\Delta CH_4{}^{cvt}} \quad (3)$$

where ΔNO_x, ΔCO^{cvt}, and $\Delta CH_4{}^{cvt}$ are the changes of each species from equation (2) and $\overline{\Delta NO_x}$, $\overline{\Delta CO^{cvt}}$, and $\overline{\Delta CH_4{}^{cvt}}$ are the changes of mean profiles from their initial values before HSS events. The resulting directly produced NO_x VMR is presented in Figure 7b with the corresponding solar wind speed in Figure 7a. The production seems to occur only above about 55-km altitude, but note that the direct production effects do not appear in January. This may result from the analysis of utilizing the tracers to remove the transport and mixing effects. The altitude range of the direct production of NO_x in this analysis seems to depend on the characteristics of downward transport and horizontal mixing of the air. In January near the SSW, the horizontal mixing occurred in the middle atmosphere and it may have eliminated even the directly produced NO_x as seen in Figure 7b. The directly produced NO_x by EEP during HSS events reaches down to about 55-km

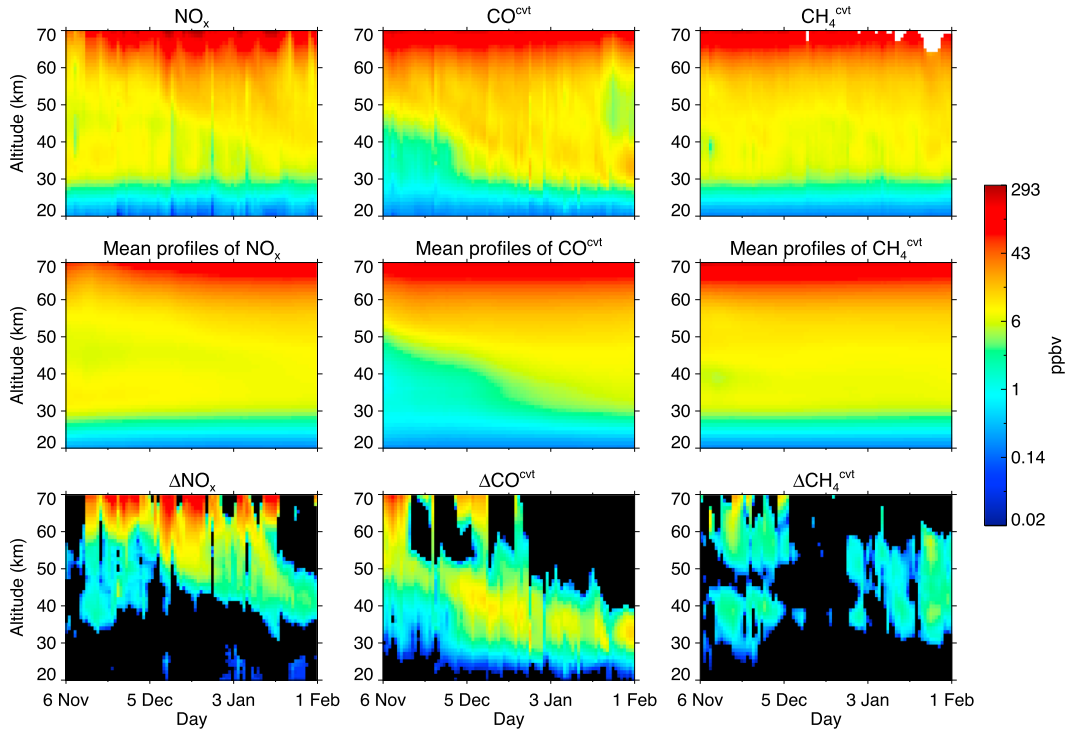

Figure 6. Vertical profiles of NO_x, converted CO, and converted CH_4 in the geomagnetic latitude of 60–77°N from 6 November 2007 to 1 February 2008, and their mean profiles are presented in the top and middle rows, respectively. The differences between two values are also presented at the bottom row.

altitude, which is consistent with the altitude range obtained by the periodogram analysis in section 3.2. The amount of NO_x by direct production is about 2 ppbv at 55-km altitude, and it increases with altitude up to about 112 ppbv at 70-km altitude. Smith-Johnsen et al. (2017) investigated the direct and indirect NO responses to the electron precipitation during the geomagnetic storm in April 2010 using the data from SOFIE instrument on board the AIM satellite. Their results show that the direct NO production was about 2 ppbv at 55-km altitude, which is similar to our result. Sinnhuber et al. (2014) also investigated the impact of energetic particle precipitation on NO_x using MIPAS data from October 2003 to March 2004 and found that the direct production of NO_x was about 3–6 ppbv at the altitude of 40–64 km.

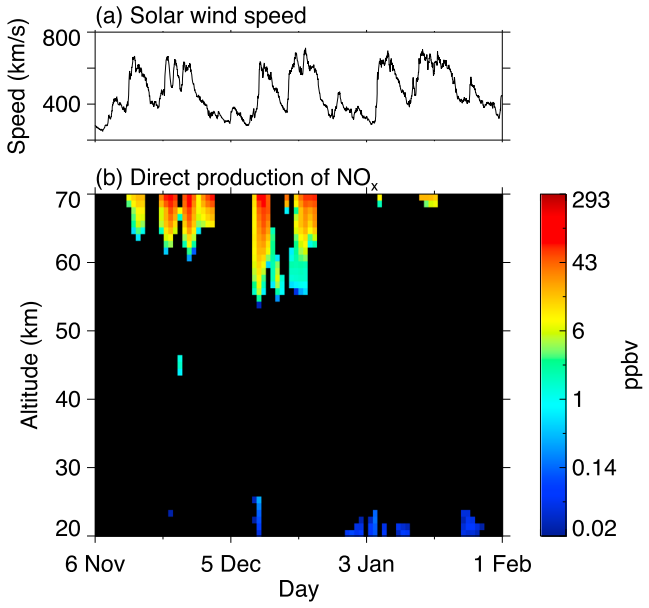

Figure 7. (a) The solar wind speed and (b) the estimation of directly produced NO_x in the Arctic winter during high-speed solar wind stream events from 6 November 2007 to 1 February 2008.

4.3. Effects on Ozone by NO_x Enhancement

In this section, we evaluate the stratospheric O_3 loss by NO_x induced by EEP during HSS events. The stratospheric O_3 destruction by EEP is mostly related to the transported NO_x from higher altitude by meridional circulation (Baumgaertner et al., 2009; Damiani et al., 2016; Randall et al., 2007). The O_3 destruction during a major SSW can also be generated by horizontal mixing of NO_x-rich air from lower latitudes (Sagi et al., 2017). In order to identify the effect on O_3 destruction by EEP-induced NO_x alone, we will focus on the period of weak horizontal mixing in December. Figure 8 shows the latitudinal variations of the mean VMRs of O_3, NO_x, CO, N_2O, and CH_4 in the altitude range of 46–49 (Figure 8a) and 30–45 km (Figure 8b). The black vertical dashed line indicates SSW onset, and the white vertical dashed lines represent the December in which we are focusing. There are clear O_3 depletions at higher latitudes in both altitude

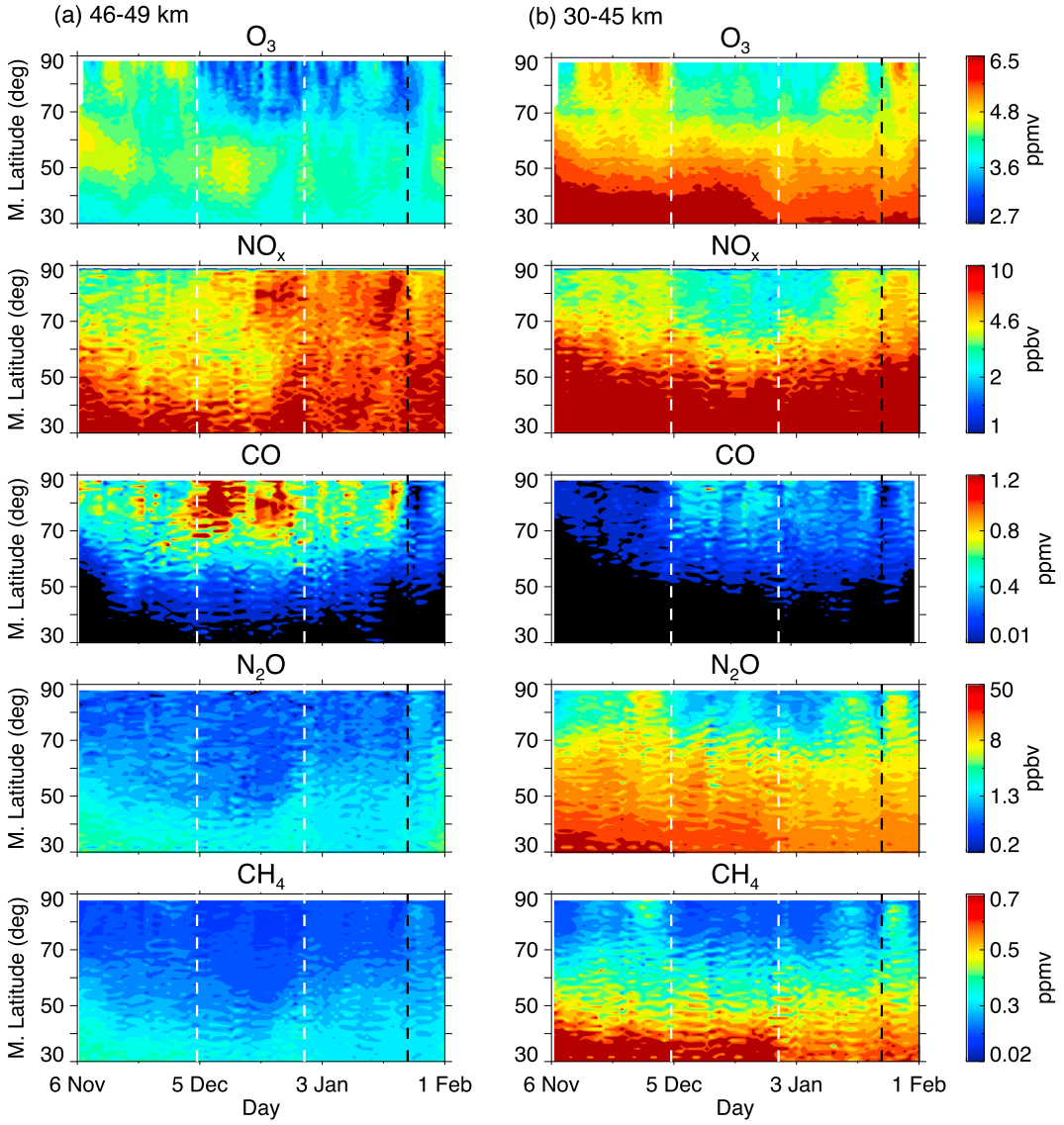

Figure 8. Daily vertical mean volume mixing ratios (a) in the altitude range of 46–49 km and (b) in the altitude range of 30–45 km for O_3, NO_x, CO, N_2O, and CH_4, in the Arctic winter from 6 November 2007 to 1 February 2008. The black vertical dashed lines indicate the stratospheric sudden warming onset and the white dashed lines indicate the December period.

regions. Note that there is a corresponding enhancement of NO_x in the upper stratosphere. This enhancement of NO_x in December can be downward transported NO_x during HSS events, which is supported by the simultaneous increase of CO and decreases of CH_4. In December, the horizontal mixing effect is very weak in CO and the N_2O VMR was very low, only about 1 ppbv. Furthermore, the NO produced by dissociation of N_2O can destroy the O_3 only at around 30-km altitude. In the lower altitude region (30–45 km), however, the O_3 depletion was accompanied by NO_x depletion, which is contradictory to the theory of EEP-induced NO_x and O_3 depletion. Therefore, it can be concluded that the effects of EEP-induced NO_x on O_3 is effective only in the upper stratosphere (46–49 km) but with no effect in the lower altitude, which is consistent with Damiani et al. (2016). It should be noted that due to the occurrence of downward transport of EEP-induced NO_x, Figure 8 provides an upper bound of ozone depletion in connection to HSS. Low concentration of ozone may occur even without catalytic NO_x-induced loss, where accurate quantification would need a data assimilation approach, which would be beyond the scope of this study.

5. Summary and Conclusion

We investigated the effects of EEP during HSSs on NO_x and O_3 in the stratosphere and the lower mesosphere, using the VMRs of the atmospheric chemical species such as CO, CH_4, NO, NO_2, and O_3 which were measured from satellite observations during the period of 6 November 2007 to 1 February 2008 (IPY 2007–2008). In this period, the overall geomagnetic activity was generally quiet and therefore electron precipitations with broad energy ranges are mostly associated with HSS events. The estimation of directly produced NO_x by EEP during HSS events was attempted by using the dynamic tracers such as CO and CH_4. The results showed that the direct production of NO_x was observed down to 55 km in spite of being as small as 2 ppbv. The produced NO_x is also consistent with HSS events during the study period. The estimated direct production of NO_x increases with altitude up to about 112 ppbv at 70-km altitude. This result indicates that the variations of polar stratospheric NO_x in winter are mostly associated with dynamical processes such as vertical transport and horizontal mixing. We also found that the O_3 depletion during HSS events seems to be related to the EEP-induced NO_x in the altitude region of 46–49 km in the polar region above about 70°N.

Acknowledgments

This work was supported by the grant PE18020 from the Korea Polar Research Institute. Y.-S. Kwak was supported by the "Operation and application researches of space weather research center" project from Korea Astronomy and Space Science Institute (KASI) and by Air Force Office of Scientific Research (AFOSR)/Asian Office of Aerospace Research and Development (AOARD) grant FA2386-18-1-0107. Y.-S. Lee acknowledges support from Chungnam National University. We would like to thank the European Space Agency (ESA) for making the MIPAS level-1b data set available at http://www.imk-asf.kit.edu/english/308.php. The MLS/Aura data are provided by the NASA Goddard Earth Sciences Data and Information Service Center (GES DISC) at http://disc.sci.gsfc.nasa.gov/Aura/data-holdings/MLS. POES data are provided by NOAA National Geophysical Data Center. The solar wind data obtained by ACE is provided at OMNIWeb/CDAWeb in the National Space Science Data Center (NSSDC), the National Aeronautics and Space Administration/Goddard Space Flight Center (NASA/GSFC).

References

Andersson, M. E., Verronen, P. T., Rodger, C. J., Clilverd, M. A., & Seppälä, A. (2014). Missing driver in the Sun-Earth connection from energetic electron precipitation impacts mesospheric ozone. *Nature Communications*, *5*(1), 5197. https://doi.org/10.1038/ncomms6197

Andersson, M. E., Verronen, P. T., Wang, S., Rodger, C. J., Clilverd, M. A., & Carson, B. R. (2012). Precipitating radiation belt electrons and enhancements of mesospheric hydroxyl during 2004–2009. *Journal of Geophysical Research*, *117*, D09304. https://doi.org/10.1029/2011JD017246

Baumgaertner, A. J. G., Jöckel, P., & Brühl, C. (2009). Energetic particle precipitation in ECHAM5/MESSy1—Part 1: Downward transport of upper atmospheric NO_x produced by low energy electrons. *Atmospheric Chemistry and Physics*, *9*(8), 2729–2740. https://doi.org/10.5194/acp-9-2729-2009

Blake, J. B., Baker, D. N., Turner, N., Ogilvie, K. W., & Lepping, R. P. (1997). Correlation of changes in the outer-zone relativistic-electron population with upstream solar wind and magnetic field measurements. *Geophysical Research Letters*, *24*(8), 927–929. https://doi.org/10.1029/97GL00859

Damiani, A., Funke, B., López Puertas, M., Santee, M. L., Cordero, R. R., & Watanabe, S. (2016). Energetic particle precipitation: A major driver of the ozone budget in the Antarctic upper stratosphere. *Geophysical Research Letters*, *43*, 3554–3562. https://doi.org/10.1002/2016GL068279

Evans, D. S., & Greer, M. S. (2004). Polar orbiting environmental satellite space environment monitor-2 instrument descriptions and archive data documentation. *NOAA Tech. Mem. 1.4*, Space Environ. Lab., Boulder, CO.

Fischer, H., Birk, M., Blom, C., Carli, B., Carlotti, M., von Clarmann, T., et al. (2008). MIPAS: An instrument for atmospheric and climate research. *Atmospheric Chemistry and Physics*, *8*(8), 2151–2188. https://doi.org/10.5194/acp-8-2151-2008

Frederick, J. E., & Orsini, N. (1982). The distribution and variability of mesospheric odd nitrogen: A theoretical investigation. *Journal of Atmospheric and Terrestrial Physics*, *44*(6), 479–488. https://doi.org/10.1016/0021-9169(82)90137-4

Funke, B., Ball, W., Bender, S., Gardini, A., Harvey, V. L., Lambert, A., et al. (2017). HEPPA-II model-measurement intercomparison project: EPP indirect effects during the dynamically perturbed NH winter 2008–2009. *Atmospheric Chemistry and Physics*, *17*(5), 3573–3604. https://doi.org/10.5194/acp-17-3573-2017

Funke, B., López-Puertas, M., Fischer, H., Stiller, G. P., von Clarmann, T., Wetzel, G., et al. (2007). Comment on "Origin of the January–April 2004 increase in stratospheric NO_2 observed in northern polar latitudes" by Jean- Baptiste Renard et al. *Geophysical Research Letters*, *34*, L07813. https://doi.org/10.1029/2006GL027518

Funke, B., López-Puertas, M., Stiller, G. P., & von Clarmann, T. (2014). Mesospheric and stratospheric NO_y produced by energetic particle precipitation during 2002–2012. *Journal of Geophysical Research: Atmospheres*, *119*, 4429–4446. https://doi.org/10.1002/2013JD021404

Gonzalez, A. L. C., & Gonzalez, W. D. (1987). Periodicities in the interplanetary magnetic field polarity. *Journal of Geophysical Research*, *92*(A5), 4357–4375. https://doi.org/10.1029/JA092iA05p04357

Gonzalez, A. L. C., Gonzalez, W. D., Dutra, S. L. G., & Tsurutani, B. T. (1993). Periodic variation in the geomagnetic activity: A study based on the *Ap* index. *Journal of Geophysical Research*, *98*(A6), 9215–9231. https://doi.org/10.1029/92JA02200

Isono, Y., Mizuno, A., Nagahama, T., Miyoshi, Y., Nakamura, T., Kataoka, R., et al. (2014). Variations of nitric oxide in the mesosphere and lower thermosphere over Antarctica associated with a magnetic storm in April 2012. *Geophysical Research Letters*, *41*, 2568–2574. https://doi.org/10.1002/2014GL059360

Jackman, C. H., McPeters, R. D., Labow, G. J., Fleming, E. L., Praderas, C. J., & Russell, J. M. (2001). Northern Hemisphere atmospheric effects due to the July 2000 solar proton event. *Geophysical Research Letters*, *28*(15), 2883–2886. https://doi.org/10.1029/2001GL013221

Kirkwood, S., Osepian, A., Belova, E., Urban, J., Perot, K., & Sinha, A. K. (2015). Ionization and NO production in the polar mesosphere during high-speed solar wind streams: Model validation and comparison with NO enhancements observed by Odin-SMR. *Annales de Geophysique*, *33*(5), 561–572. https://doi.org/10.5194/angeo-33-561-2015

Lam, M. M., Horne, R. B., Meredith, N. P., Glauert, S. A., Moffat-Griffin, T., & Green, J. C. (2010). Origin of energetic electron precipitation >30 keV into the atmosphere. *Journal of Geophysical Research*, *115*, A00F08. https://doi.org/10.1029/2009JA014619

Lei, J., Thayer, J. P., Forbes, J. M., Sutton, E. K., & Nerem, R. S. (2008). Rotating solar coronal holes and periodic modulation of the upper atmosphere. *Geophysical Research Letters*, *35*, L10109. https://doi.org/10.1029/2008GL033875

Livesey, N. J., Read, W. G., Froidevaux, L., Lambert, A., Manney, G. L., Pumphrey, H. C., et al. (2011). EOS MLS version 3.3 level 2 data quality and description document. *Jet Propulsion Laboratory* (JPL D-33509, Version 3.3x-1.0). Retrieved from https://mls.jpl.nasa.gov/data/v3-3_data_quality_document.pdf

López-Puertas, M., Funke, B., Gil-Lopez, S., von Clarmann, T., Stiller, G. P., Hopfner, M., et al. (2005). Observation of NO_x enhancement and ozone depletion in the Northern and Southern Hemispheres after the October–November 2003 solar proton events. *Journal of Geophysical Research*, *110*, A09S43. https://doi.org/10.1029/2005JA011050

McComas, D. J., Bame, S. J., Barker, P., Feldman, W. C., Phillips, J. L., Riley, P., & Griffee, J. W. (1998). Solar Wind Electron Proton Alpha Monitor (SWEPAM) for the Advanced Composition Explorer. *Space Science Reviews*, *86*(1/4), 563–612. https://doi.org/10.1023/A:1005040232597

McElroy, M. B., & McConnell, J. C. (1971). Nitrous oxide: A natural source of stratospheric NO. *Journal of the Atmospheric Sciences*, *28*(6), 1095–1098. https://doi.org/10.1175/1520-0469(1971)028<1095:NOANSO>2.0.CO;2

Meredith, N. P., Horne, R. B., Lam, M. M., Denton, M. H., Borovsky, J. E., & Green, J. C. (2011). Energetic electron precipitation during high-speed solar wind stream driven storms. *Journal of Geophysical Research*, *116*, A05223. https://doi.org/10.1029/2010JA016293

Minschwaner, K., Manney, G. L., Livesey, N. J., Pumphrey, H. C., Pickett, H. M., Froidevaux, L., et al. (2010). The photochemistry of carbon monoxide in the stratosphere and mesosphere evaluated from observations by the Microwave Limb Sounder on the Aura satellite. *Journal of Geophysical Research*, *115*, D13303. https://doi.org/10.1029/2009JD012654

Mursula, K., & Zieger, B. (1996). The 13.5-day periodicity in the Sun, solar wind and geomagnetic activity: The last three solar cycles. *Journal of Geophysical Research*, *101*(A12), 27,077–27,090. https://doi.org/10.1029/96JA02470

Nayar, S. R. P., Radhika, V. N., Revathy, K., & Ramadas, V. (2002). Wavelet analysis of solar wind and geomagnetic parameter. *Solar Physics*, *208*(2), 359–373. https://doi.org/10.1023/A:1020565831926

Newnham, D. A., Espy, P. J., Clilverd, M. A., Rodger, C. J., Seppälä, A., Maxfield, D. J., et al. (2011). Direct observations of nitric oxide produced by energetic electron precipitation into the Antarctic middle atmosphere. *Geophysical Research Letters*, *38*, L20104. https://doi.org/10.1029/2011GL048666

Nieder, H., Winkler, H., Marsh, D. R., & Sinnhuber, M. (2014). NO_x production due to energetic particle precipitation in the MLT region: Results from ion chemistry model studies. *Journal of Geophysical Research: Space Physics*, *119*, 2137–2148. https://doi.org/10.1002/2013JA019044

O'Brien, T. P., Looper, M. D., & Blake, J. B. (2004). Quantification of relativistic electron microburst losses during the GEM storms. *Geophysical Research Letters*, *31*, L04802. https://doi.org/10.1029/2003GL018621

Pickett, H. M., Read, W. G., Lee, K. K., & Yung, Y. L. (2006). Observation of night OH in the mesosphere. *Geophysical Research Letters*, *33*, L19808. https://doi.org/10.1029/2006GL026910

Porter, H. S., Jackman, C. H., & Green, A. E. S. (1976). Efficiencies for production of atomic nitrogen and oxygen by relativistic proton impact in air. *The Journal of Chemical Physics*, *65*(1), 154–167. https://doi.org/10.1063/1.432812

Randall, C. E., Harvey, V. L., Singleton, C. S., Bailey, S. M., Bernath, P. F., Codrescu, M., et al. (2007). Energetic particle precipitation effects on the Southern Hemisphere stratosphere in 1992–2005. *Journal of Geophysical Research*, *112*, D08308. https://doi.org/10.1029/2006JD007696

Randall, C. E., Harvey, V. L., Siskind, D. E., France, J., Bernath, P. F., Boone, C. D., & Walker, K. A. (2009). NO_x descent in the Arctic middle atmosphere in early 2009. *Geophysical Research Letters*, *36*, L18811. https://doi.org/10.1029/2009GL039706

Renard, J.-B., Blelly, P.-L., Bourgeois, Q., Chartier, M., Goutail, F., & Orsolini, Y. J. (2006). Origin of the January–April 2004 increase in stratospheric NO_2 observed in the northern polar latitudes. *Geophysical Research Letters*, *33*, L11801. https://doi.org/10.1029/2005GL025450

Rodger, C. J., Carson, B. R., Cummer, S. A., Gamble, R. J., Clilverd, M. A., Green, J. C., et al. (2010). Contrasting the efficiency of radiation belt losses caused by ducted and non-ducted whistler mode waves from ground-based transmitters. *Journal of Geophysical Research*, *115*, A12208. https://doi.org/10.1029/2010JA015880

Rodger, C. J., Clilverd, M. A., Green, J. C., & Lam, M. M. (2010). Use of POES SEM-2 observations to examine radiation belt dynamics and energetic electron precipitation into the atmosphere. *Journal of Geophysical Research*, *115*, A04202. https://doi.org/10.1029/2008JA014023

Rohen, G., von Savigny, C., Sinnhuber, M., Llewellyn, E. J., Kaiser, J. W., Jackman, C. H., et al. (2005). Ozone depletion during the solar proton events of October/November 2003 as seen by SCIAMACHY. *Journal of Geophysical Research*, *110*, A09S39. https://doi.org/10.1029/2004JA010984

Rusch, D. W., Gérard, J.-C., Solomon, S., Crutzen, P. J., & Reid, G. C. (1981). The effect of particle precipitation events on the neutral and ion chemistry of the middle atmosphere—I. Odd nitrogen. *Planetary and Space Science*, *29*(7), 767–774. https://doi.org/10.1016/0032-0633(81)90048-9

Sagi, K., Pérot, K., Murtagh, D., & Orsolini, Y. (2017). Two mechanisms of stratospheric ozone loss in the Northern Hemisphere, studied using data assimilation of Odin/SMR atmospheric observations. *Atmospheric Chemistry and Physics*, *17*(3), 1791–1803. https://doi.org/10.5194/acp-17-1791-2017

Semeniuk, K., Fomichev, V. I., McConnell, J. C., Fu, C., Melo, S. M. L., & Usoskin, I. G. (2011). Middle atmosphere response to the solar cycle in irradiance and ionizing particle precipitation. *Atmospheric Chemistry and Physics*, *11*(10), 5045–5077. https://doi.org/10.5194/acp-11-5045-2011.

Seppälä, A., Verronen, P. T., Kyrölä, E., Hassinen, S., Backman, L., Hauchecorne, A., et al. (2004). Solar proton events of October–November 2003: Ozone depletion in the Northern Hemisphere polar winter as seen by GOMOS/Envisat. *Geophysical Research Letters*, *31*, L19107. https://doi.org/10.1029/2004GL021042

Sinnhuber, M., Funke, B., von Clarmann, T., López-Puertas, M., Stiller, G. P., & Seppala, A. (2014). Variability of NO_x in the polar middle atmosphere from October 2003 to March 2004: Vertical transport vs. local production by energetic particles. *Atmospheric Chemistry and Physics*, *14*(14), 7681–7692. https://doi.org/10.5194/acp-14-7681-2014

Sinnhuber, M., Nieder, H., & Wieters, N. (2012). Energetic particle precipitation and the chemistry of the mesosphere/lower thermosphere. *Surveys in Geophysics*, *33*(6), 1281–1334. https://doi.org/10.1007/s10712-012-9201-3

Sinnhuber, M., Wieters, N., & Winkler, H. (2013). The impact of energetic particle precipitation on the chemical composition of the middle atmosphere: Measurements and model predictions. In F. J. Lübken (Ed.), *Climate and Weather of the Sun-Earth System (CAWSES) Springer Atmospheric Sciences*, (pp. 275–299). Dordrecht, Netherlands: Springer. https://doi.org/10.1007/978-94-007-4348-9_16

Siskind, D. E., Barth, C. A., Evans, D. S., & Roble, R. G. (1989). The response of thermospheric nitric oxide to an auroral storm: 2. Auroral latitudes. *Journal of Geophysical Research*, *94*(A12), 16,899–16,911. https://doi.org/10.1029/JA094iA12p16899

Siskind, D. E., & Russell, J. M. III (1996). Coupling between middle and upper atmospheric NO: Constraints from HALOE observations. *Geophysical Research Letters*, *23*(2), 137–140. https://doi.org/10.1029/95GL03782

Smith-Johnsen, C., Tyssøy, H. N., Hendrickx, K., Orsolini, Y., Kumar, G. K., Ødegaard, L.-K. G., et al. (2017). Direct and indirect electron precipitation effect on nitric oxide in the polar middle atmosphere, using a full-range energy spectrum. *Journal of Geophysical Research: Space Physics*, *122*, 8679–8693. https://doi.org/10.1002/2017JA024364

Solomon, S., Barth, C. A., & Bailey, S. M. (1999). Auroral production of nitric oxide measured by the SNOE satellite. *Geophysical Research Letters*, *26*(9), 1259–1262. https://doi.org/10.1029/1999GL900235

Solomon, S., Roble, R. G., & Crutzen, P. J. (1982). Photochemical coupling between the thermosphere and the lower atmosphere I. Odd nitrogen from 50 to 120 km. *Journal of Geophysical Research*, *87*(C9), 7206–7220. https://doi.org/10.1029/JC087iC09p07206

Solomon, S., Rusch, D. W., Gerard, J.-C., Reid, G. C., & Crutzen, P. J. (1981). The effect of particle precipitation events on the neutral and ion chemistry of the middle atmosphere: II. Odd hydrogen. *Planetary and Space Science*, *29*(8), 885–893. https://doi.org/10.1016/0032-0633(81)90078-7

Swider, W., & Keneshea, T. J. (1973). Decrease of ozone and atomic oxygen in the lower mesosphere during a PCA event. *Planetary and Space Science*, *21*(11), 1969–1973. https://doi.org/10.1016/0032-0633(73)90126-8

Tsurutani, B. T., Gonzalez, W. D., Guarnieri, F., Kamide, Y., Zhou, X., & Arballo, J. K. (2004). Are high-intensity long-duration continuous *AE* activity (HILDCAA) events substorm expansion events? *Journal of Atmospheric and Terrestrial Physics*, *66*(2), 167–176. https://doi.org/10.1016/j.jastp.2003.08.015

Turunen, E., Kero, A., Verronen, P. T., Miyoshi, Y., Oyama, S.-I., & Saito, S. (2016). Mesospheric ozone destruction by high-energy electron precipitation associated with pulsating aurora. *Journal of Geophysical Research: Atmospheres*, *121*, 11,852–11,861. https://doi.org/10.1002/2016JD025015

Verkhoglyadova, O. P., Wang, S., Mlynczak, M. G., Hunt, L. A., & Zank, G. P. (2015). Effects of two large solar energetic particle events on middle atmosphere nighttime odd hydrogen and ozone content: Aura/MLS and TIMED/SABER measurements. *Journal of Geophysical Research: Space Physics*, *120*, 12–29. https://doi.org/10.1002/2014JA020609

Verronen, P. T., & Lehmann, R. (2013). Analysis and parameterisation of ionic reactions affecting middle atmospheric HO_x and NO_y during solar proton events. *Annales de Geophysique*, *31*(5), 909–956. https://doi.org/10.5194/angeo-31-909-2013

Verronen, P. T., Seppälä, A., Clilverd, M. A., Rodger, C. J., Kyrölä, E., Enell, C.-F., et al. (2005). Diurnal variation of ozone depletion during the October–November 2003 solar proton events. *Journal of Geophysical Research*, *110*, A09S32. https://doi.org/10.1029/2004JA010932

Wang, L., & Alexander, M. J. (2009). Gravity wave activity during stratospheric sudden warmings in the 2007–2008 Northern Hemisphere winter. *Journal of Geophysical Research*, *114*, D18108. https://doi.org/10.1029/2009JD011867

Waters, J. W., Froidevaux, L., Harwood, R. S., Jarnot, R. F., Pickett, H. M., Read, W. G., et al. (2006). The Earth Observing System Microwave Limb Sounder (EOS MLS) on the Aura satellite. *IEEE Transactions on Geoscience and Remote Sensing*, *44*(5), 1075–1092. https://doi.org/10.1109/TGRS.2006.873771

Yahnin, A. G., Yahnina, T. A., Semenova, N. V., Gvozdevsky, B. B., & Pashin, A. B. (2016). Relativistic electron precipitation as seen by NOAA POES. *Journal of Geophysical Research: Space Physics*, *121*, 8286–8299. https://doi.org/10.1002/2016JA022765